IEEE Access
Multidisciplinary | Rapid Review | Open Access Journal

Received August 19, 2021, accepted September 8, 2021, date of publication September 13, 2021, date of current version October 26, 2021.

Digital Object Identifier 10.1109/ACCESS.2021.3112128

Random Interleaving Multiplexing Based IRSA Random Access System for Satellite-Enabled Internet-of-Things

JIAN DING[1,2], JINGRUI SU[1], (Graduate Student Member, IEEE), CONG LI[3], GUANGLIANG REN[1], (Member, IEEE), AND HAO WANG[1]

[1]State Key Laboratory of Integrated Services Networks, Xidian University, Xi'an 710071, China
[2]National Key Laboratory of Electromagnetic Environment, China Research Institute of Radiowave Propagation, Qingdao 266107, China
[3]Academy of Space Electronic Information Technology, Xi'an 710100, China

Corresponding author: Guangliang Ren (glren@mail.xidian.edu.cn)

This work was supported in part by the National Natural Science Foundation of China under Grant 91538105 and Grant 61801352.

ABSTRACT A random access framework based on random interleaving multiplexing (RIM) is proposed to further improve throughput for internet of things in satellite networks, which resort to the state-of-art physical layer techniques that can resolve multiple packet collisions issue. The interleavers are randomly selected by active devices from a set of available interleavers, which are used to differentiate signals of different devices sharing a subframe that consists of multiple time slots. The message passing detector (MPD) is utilized to decode collided packets. By means of transmission diversity and interference cancellation, the proposed scheme can be linked with the irregular repetition slotted ALOHA (IRSA), the RIM-IRSA protocol is proposed. The analysis of packet loss ratio (PLR) of the RIM-IRSA is given by using the density evolution method, and the optimal degree distributions are given. Simulation results show that the RIM-IRSA outperforms traditional IRSA protocol.

INDEX TERMS Satellite networks, random access (RA), random interleaving multiplexing (RIM), irregular repetition slotted ALOHA (IRSA), message passing algorithm (MPA).

I. INTRODUCTION

With the development of the Internet of Things (IoT) in wireless communication technology and satellite communication networks, satellite-enabled IoTs gradually attract much more attentions since they have tremendous broad coverage and support various applications scenarios [1], [2]. A massive number of devices in a beam coverage area require to access to the satellite node, which have brought in a challenge to the access system in satellite-enabled IoTs. The network is characterized by a large number of devices and short packets, which makes the grant-based multiple access techniques inefficient, such as time division multiple addresses (TDMA), multi-frequency (MF)-TDMA, and demand assignment multiple access (DAMA) [3]. The traffic requirement of IoT can be well satisfied by grant free random access (RA) techniques for this technique have uncoordinated and competitive characteristics [4], [5].

The associate editor coordinating the review of this manuscript and approving it for publication was Nan Wu.

A. RELATED LITERATURES

ALOHA-based RA schemes are well suitable for IoT and wireless sensor networks (WSNs) due to their uncoordinated and simple nature. Slotted ALOHA (SA) is first proposed as an uplink RA scheme, in which every active device transmits its only one packet to an access point in a randomly selected time slot. SA is a simple RA scheme for WSNs, but packet collisions and high packet loss ratio (PLR) have become the main limitation. In [6], the diversity slotted ALOHA (DSA) scheme can be viewed as a slightly enhanced version to slotted ALOHA (SA), a tiny throughput performance improvement at low traffic load compared with SA by allowing every sensor devices to transmit two replicas of the same burst instead of one. Similarly to DSA, the contention resolution diversity slotted ALOHA (CRDSA) [7] scheme transmits two packet replicas on randomly selected two slots within a TDMA frame in satellite network. However, the CRDSA scheme can utilize the location pointer of packet replicas and the iterative interference cancellation (IC) technique to clear up some interference caused by replicas. Thanks to applying

simple yet effective IC technique and accurate channel estimation, CRDSA achieve higher throughput and lower PLR compared to SA and DSA. To further improve the performance of CRDSA, the CRDSA++ scheme is proposed in [8], in which every device transmits multiple packet replicas (i.e., 3, 4, 5) in a TDMA frame to increase the probability of packet successful transmission. However, CRDSA-3 is testified that it is the most effective and throughput in the CRDSA-like scheme. To further improve the existing RA schemes comprising CRDSA and CRDSA++, in [9], irregular repetition slotted ALOHA (IRSA) is proposed, which relies on a bipartite graph optimization by establishing a relationship between IC process and the decoding process of bipartite graph-based low-density parity-check (LDPC) codes. In the IRSA scheme, every active device transmits the irregular number of packet replicas according to optimal probability mass function (PMF). Therefore, IRSA can dramatically improve performance compared to CRDSA and CRDSA++ schemes that can be viewed as a special case with regular graphs. In the mentioned above advanced protocols, the peak normalized throughput is about 0.8 packets/slot.

To further improve the throughput of RA schemes, some new schemes are proposed to resolve multiple packet collisions issue, such as those in literature [10]–[15]. In [10], the authors propose an IRSA with energy harvesting nodes RA protocol. In [11], authors further enhance the IRSA scheme performance by considering the received replica power imbalance due to the natural dispersion and open-loop power control mechanism. In [12], multi-power IRSA is proposed, in which receiver use the capture effect to enhances the protocol performance. The NOMA-based IRSA is proposed for satellite networks in [13], in which apply NOMA technique to IRSA can outperform existing traditional IRSA schemes, and optimal degree distributions at different discrete power level are derived by employing differential evolution algorithm. However, the NOMA based IRSA-like schemes have high energy consumption for a large number of devices with have limited battery life and power consumption. The sizable energy consumption will affect the lifetime of the whole IoTs and be detrimental to the ecology environment from the perspective of green communications. In [14], the polarized MIMO based IRSA scheme is proposed by utilizing polarization characteristic of satellite link and MIMO detection in satellite networks. Although the throughput can be improved, the scheme is difficult to deploy for devices without polarized antennas. The authors in [15] proposed the Q-learning based IRSA scheme, however it cannot be applied into the satellite-enabled IoTs because of the delay problem caused by online learning. From the perspective of code-domain non-orthogonal multiple access (NOMA), we utilized the interleaver randomly selected to distinguish different users and proposed a random interleaving multiplexing based CRDSA protocol in [16]. The protocol can achieve a high throughput, but it also has high detection complexity and the employed CRDSA protocol is inferior to IRSA protocol, and the proposed RA scheme is far from perfect. This has motivated us to further investigate and expand the idea in [16], and analyze its performance.

B. CONTRIBUTIONS OF THE WORK

To further improve the throughput of RA scheme and without increasing its energy consumption, we propose a random interleaving multiplexing based RA framework and employ the advanced protocol for IoT-oriented satellite networks. The main contributions of this paper are summarized as follows.

1) We propose a novel RIM based RA framework to expand the idea in [16] for IoT-oriented satellite networks, which employs interleavers to differentiate data from different devices being multiplexed in a sub-frame consisting of multiple slots. The packets of each active device are interleaved by a randomly selected interleaver and are mapped onto a sub-frame. The multiple superimposed packets can be successfully decoded by utilizing the message passing detector (MPD).
2) A theoretical analysis framework to evaluate the performance of the proposed scheme is developed. The collision probability of preambles and interleavers are derived, and the performance of the proposed scheme is analyzed.
3) We utilize a subframe with the RIM as an elementary transmission unit; and combine with IRSA, which generates the RIM-IRSA protocol. Particularly, the detailed procedures of active devices and satellite nodes in the RIM-IRSA protocol are specified, and its probability mass function is also optimized due to the different transmission scheme in physical layer.

The rest of this paper is organized as follows. In Section II, we present the system model. The proposed framework is presented in section III. The RIM-IRSA protocol is presented in section IV. In Section V, the performance analysis of the RIM-IRSA protocol is presented. In section VI, the computer simulation results are presented. In section VII, the conclusion is presented.

II. SYSTEM OVERVIEW

The satellite-enabled IoTs contains a low earth orbit (LEO) satellite and a geosynchronous earth orbit (GEO) satellite node, massive devices and the gateway stations. Massive devices sporadically activated with an activation probability transmit packets to the satellite, then the satellite further relays received packets to the ground gateway station, which can decode the received signals and relays acknowledgement bits to devices via the satellite node. In satellite-enabled IoTs, we assume that all devices synchronously and competitively access into the satellite nodes. The system model of the satellite-enabled IoTs is shown in Fig.1.

It is considered that the single-carrier interleaved frequency division multiple access (SC-IFDMA) is used to carry the signals in the transmission packet transmit by devices, because SC-IFDMA has low peak-to-average power ratio (PAPR) and constant envelope. In addition, each device access into the satellite by share the same bandwidth resource.

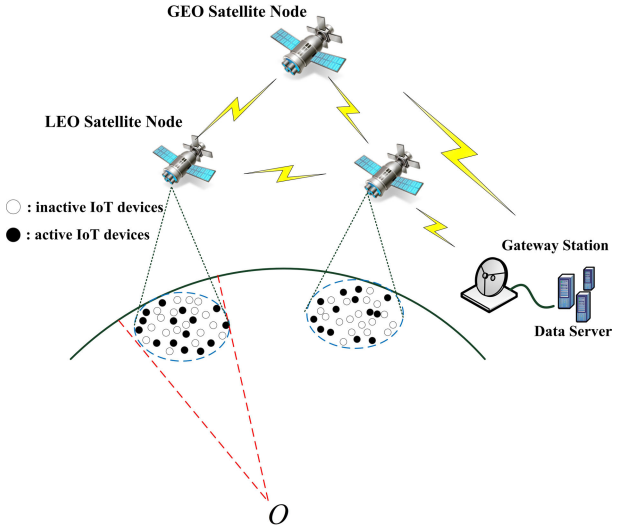

FIGURE 1. System model of satellite-enabled IoTs.

Denoted by T_F the duration of a MAC frame, which is composed of N_{slot} time slots, and denoted by $T_S = T_F/N_{slot}$ the duration of one slot. The number of activated devices in a MAC frame can be modeled as a Poisson random variable, which is defined as $U \sim Po(\lambda)$, where $Po(\cdot)$ denotes a Poisson distribution and is the average packet arrival rate, which can be calculated as

$$\lambda = N_{slot}G, \tag{1}$$

where G denotes the normalized load.

In addition, the PLR can be defined as the ratio of the number of incorrectly decoded or lost packets to the total number of sent packets, therefore the PLR is closely relative to the normalized load G. The normalized throughput T can be defined as the ratio of the number of successfully transmitted devices to the total number of devices. The normalized throughput T can also expressed as $T(G) = G\cdot[1-PLR(G)]$.

III. PROPOSED RIM BASED RANDOM ACCESS FRAMEWORK

In this section, we present the proposed framework of RIM based random access, including the structure resource block and interleaving mapping of packet, transmitted and received signal model of interleaving based packet, preamble and interleaver detection and multiple user detection.

A. RANDOM INTERLEAVING MULTIPLEXING

In the proposed RIM scheme, a sub-frame can be viewed as the basic transmission unit, which can consist of multiple time slots. We assume that a MAC frame is divided to N_{sf} sub-frame, which each sub-frame consists of L slots. The structure of the frame in proposed scheme can be shown in Fig.2.

By using interleaving domain NOMA scheme [8], the RIM based RA scheme can be proposed which can further improve the availability of the single slot (i.e., multiple packets in a slot can be successfully decoded) and resolve the so-called

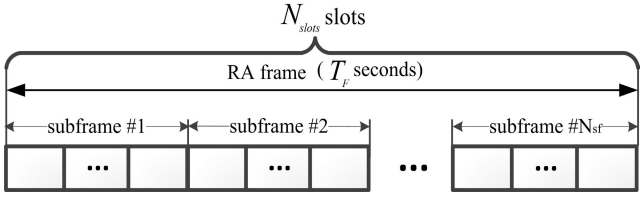

FIGURE 2. Structure of frame.

deadlock loop problem. We assume that each burst includes of k information bits, then each burst can be encoded by the forward error correcting (FEC) code with code rate r. The coded sequence of the u^{th} device can be expressed as $\boldsymbol{x}_u = [x_{u,1}, x_{u,2}, x_{u,3}, \ldots, x_{u,k'}]$ ($k' = k/r$ denotes the length of coded sequence). Then the coded sequence of the u^{th} device can be interleaved by a bit level interleaver randomly selected from the set $\Psi_b = [\boldsymbol{I}_1^b, \ldots, \boldsymbol{I}_u^b, \ldots, \boldsymbol{I}_{V_b}^b]$, where permutation matrix $\boldsymbol{I}_u^b \in C^{k'\times k'}$ indicates an interleaver. If the chosen interleaver by the u^{th} device is $\boldsymbol{I}_u^b$, the interleaved sequence in the i^th subframe of the device u^{th} can be denoted as

$$\boldsymbol{s}_i^u = \boldsymbol{I}_u^b \boldsymbol{x}_u. \tag{2}$$

The interleaved sequence of the u^{th} device then can be modulated with the modulation order O. Therefore, the symbol sequence of the u^{th} device is represented as $\tilde{\boldsymbol{s}}_i^u = [s_{u,1}, s_{u,2}, s_{u,3}, \ldots, s_{u,n}]$ ($n = k'/\log_2(O)$ denotes the length of symbol sequence). Then all activated devices can be further perform zero padding and symbol level interleaving process. In zero padding process, we can define a density parameter ρ as $\rho = L_{used}/L_{all}$, where L_{used} and L_{all} are the number of the actually occupied slot and the number of the overall assigned slot for each device, respectively. By selecting various value of density parameter, different level of diversity order can be used and ρ decides the number of padded zero value. In proposed scheme, the L_{used} and L_{all} can be selected as 1 and the number of slots in a sub-frame L. The symbol sequence is then interleaved by a symbol level interleaver selected from the set $\Psi_s = [\boldsymbol{I}_1^s, \ldots, \boldsymbol{I}_u^s, \ldots, \boldsymbol{I}_{V_s}^s]$, where permutation matrix $\boldsymbol{I}_u^s \in C^{n\times n}$ indicates a interleaver. It is assumed that the randomly chosen interleaver by the u^{th} device is $\boldsymbol{I}_u^s$, the interleaved bit signal can be denoted as

$$\boldsymbol{S}_i^u = \boldsymbol{I}_u^s \boldsymbol{s}_i^u = \boldsymbol{I}_u^s \boldsymbol{I}_u^b \boldsymbol{x}_u. \tag{3}$$

In Fig.3, an example of symbol level interleaving procedure for $\rho = 0.5$ is shown. The modulated symbols of each device are mapped onto a portion of sub-frames of an allocated resource grid. As shown in Fig.4, a performing process diagram of transmitter of RIM scheme is considered. In dark blue modified blocks are unique ones in proposed scheme.

The preamble or postamble not only can be used to recognize user activity and estimate channel parameters in RA process, but also employ to recognize the bit level and symbol level interleavers that are randomly chosen by the u^{th} device in the proposed scheme. We use Zadaoff-Chu as

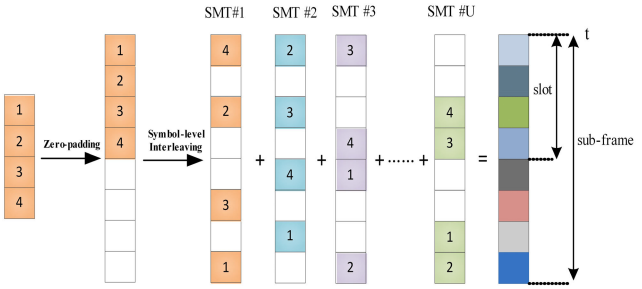

FIGURE 3. Example of grid mapping process when $N = 4$, $\rho = 0.5$ and $L = 8$.

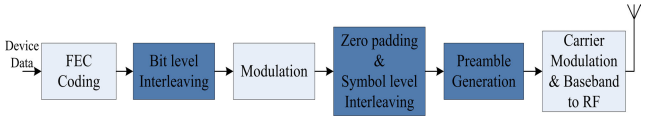

FIGURE 4. The block diagram of transmitter of RIM scheme.

preambles and postambles because of good auto- and cross-correlation properties. The sets of bit level and symbol level interleavers are defined by $\Phi_b = [\boldsymbol{P}_1^{pre}, \ldots, \boldsymbol{P}_\eta^{pre}, \ldots, \boldsymbol{P}_{V_b}^{pre}]$ and $\Phi_s = [\boldsymbol{P}_1^{pos}, \ldots, \boldsymbol{P}_v^{pos}, \ldots, \boldsymbol{P}_{V_s}^{pre}]$, where the V_b and V_s denote respectively the number of preamble and postamble in the their own sets. Note that every preamble and postamble are in association with every bit level and symbol level interleaver. It is assumed that the length of a preamble and postamble is L_p^{RA}.

B. SIGNAL MODEL OF A PACKET

The SC-IFDMA symbol is utilized to transmit the packets from devices due to its advantage of low PAPR and constant envelop characteristics, so it is suitable for satellite-enabled IoTs with a high power efficiency.

We assume that the transmitted data of the m^{th} SC-IFDMA symbol in the i subframe of the u^{th} device can be indicated as $\boldsymbol{s}_i^u(m) = [s_i^u(m,0), s_i^u(m,1), \ldots, s_i^u(m,M-1)]^T$, where M is the number of modulated data of one SC-IFDMA symbol of the u^{th} device and $\{\cdot\}^T$ denotes the transpose of $\{\cdot\}$. After an M point discrete Fourier transform (DFT), the signal of the u^{th} device in the frequency domain can be indicated as

$$\boldsymbol{S}_i^u(m) = \boldsymbol{F}_M \boldsymbol{s}_i^u(m), \tag{4}$$

where $\boldsymbol{S}_i^u(m) = [\boldsymbol{S}_i^u(m,0), \boldsymbol{S}_i^u(m,1), \ldots, \boldsymbol{S}_i^u(m,M-1)]^T$, and $\boldsymbol{F}_M$ is the DFT matrix with dimension of M, in which the element in the $(R,C)^{th}$ is $\boldsymbol{F}_M(R,C) = \exp(-j2\pi RC/M)/\sqrt{M}$. The interleaved subcarrier mapping can be carried out to make the vector $\boldsymbol{S}_i^u(m)$ distribute uniformly in the available N subcarriers, where $N = V \cdot Z$, and V denotes spreading factor. The mapped signal vector $\boldsymbol{S'}_i^u(m)$ is indicated as

$$\boldsymbol{S'}_i^u(m) = Q\boldsymbol{S}_i^u(m), \tag{5}$$

where Q is a $N \times M$ mapping matrix of which $(n,m)^{th}$ element is 1 when the data on the m^{th} subcarrier is mapped to the n^{th} subcarrier, otherwise the element are 0. After an N point inverse DFT (IDFT) for vector $\boldsymbol{S'}_i^u(m)$, the signal vector $\boldsymbol{x}_i^u(m)$ in time-domain is indicated as

$$\boldsymbol{x}_i^u(m) = \boldsymbol{F}_N^{-1} \boldsymbol{S'}_i^u(m), \tag{6}$$

where $\boldsymbol{x}_i^u(m) = [\boldsymbol{x}_i^u(m,0), \boldsymbol{x}_i^u(m,0), \ldots, \boldsymbol{x}_i^u(m,N-1)]^T$, and $\boldsymbol{F}_N^{-1}$ indicates IDFT matrix with N, in which the element in the $(E,J)^{th}$ is $\boldsymbol{F}_N^{-1}(E,J) = \exp(j2\pi EJ/N)/\sqrt{N}$. Finally, cyclic prefix (CP) is put into vector $\boldsymbol{x}_i^u(m)$, so the transmitted signal vector can be indicated as

$$\begin{aligned} &P_i^u(m) \\ &= [x_i^u(m, N-L_{cp}), x_i^u(m, N-L_{cp}+1), \ldots, x_i^u(m, N-1), \\ &\quad \times x_i^u(m,0), x_i^u(m,1), \ldots, x_i^u(m, N-1)]^T, \end{aligned} \tag{7}$$

where L_{cp} is the length of CP, then the length of m^{th} SC-IFDMA symbol is $N + L_{cp}$.

Each transmitted packet contains preamble, payload with L_{pay} SC-IFDMA and postamble blocks, respectively. $\boldsymbol{S}_i^u$ is the transmitted signal in i^{th} subframe of a packet generated by the u^{th} user, which can be represented as

$$\boldsymbol{S}_i^u = [\boldsymbol{P}_\eta^{pre}, \boldsymbol{P}_i^u(1), \ldots, \boldsymbol{P}_i^u(1), \ldots \boldsymbol{P}_i^u(L), \boldsymbol{P}_v^{pos}]. \tag{8}$$

where $S_u(l)(l \in [1, L_{pkt}^{RA}])$ is the l^{th} transmitted symbol of the u^{th} device.

We assume that the number of the devices in the i^{th} subframe is U_i. The $k^{th}(k \in [1, \ldots, L_{pkt}^{RA}])$ received symbol in the i^{th} subframe can be expressed as

$$\boldsymbol{Y}_i(k) = \sum_{u=1}^{U_i} h_i^u \boldsymbol{S}_i^u(k) z^{-\tau_{u,i}} + \boldsymbol{W}_i(k), \tag{9}$$

where h_i^u and $\tau_{u,i}$ represent the channel coefficient and propagation delay of the u^{th} device in the i^{th} subframe, respectively. The channel model that from devices to the satellite can be modeled as the Rician channel, and $z^{-\tau_{u,i}}$ denotes the delay operator that shifts rightward the received signal by $\tau_{u,i}$. $\boldsymbol{W_i}$ represents the matrix of Addition White Gaussian Noise (AWGN) with zero mean and σ^2 variance.

C. PREAMBLE AND INTERLEAVING DETECTION

When the gateway receives a frame signal, preambles detection be firstly performed to confirm the number of devices in each subframe and their chosen interleaver, then parameters estimation is performed to estimate their channel coefficients. In the i^{th} subframe, by correlating the received preamble and postamble signals with local preambles and postambles, we can have

$$\begin{aligned} I_i^{pre} &= \arg\max_\tau \{|\boldsymbol{p}_\eta^{pre} \cdot \boldsymbol{Y}_i^H[\tau : \tau + L_p^{RA}]|\} \\ I_i^{pos} &= \arg\max_\tau \{|\boldsymbol{p}_v^{pos} \cdot \boldsymbol{Y}_i^H[L' : L' + L_p^{RA}]|\} \\ \eta &= 1, \ldots, V_b; v = 1, \ldots, V_s \end{aligned} \tag{10}$$

where $\boldsymbol{Y}_i[\tau : \tau + L_p^{RA}]$ and $\boldsymbol{Y}_i[L' : L' + L_p^{RA}]$ $(L' = \tau + L_p^{RA} + L_{sc}(N + L_{cp}))$ represent respectively the preamble and postamble vector extracted from $\boldsymbol{Y}_i$. $\tau = 1, \ldots, \tau_{\max}$ is the indices of symbols offset and $\tau_{\max}$ is the maximum offset. If $\left|I_i^{pre}(\tau)/L_p^{RA}\right| > \gamma$ and $\left|I_i^{pos}(\tau)/L_p^{RA}\right| > \gamma$, the preamble and postamble can be viewed respectively as active preamble and postamble, where γ presents a predefined threshold about preamble and postamble detection.

Note that if some devices reuse the same preamble, the devices still possible can be distinguished as long as the preamble has different frequency and timing offsets. By traversing all preambles in each subframe, we can obtain the number of devices and their chosen interleavers.

D. MESSAGE PASSING ALGORITHM DETECTOR (MPAD) FOR SUPERIMPOSED PACKET

By using the low-complexity sub-optimal MPA detection algorithm, MPAD can make it possible to decode multiple collided replicas [20]–[22]. The number of active users in a subframe is stochastic because of the RA nature. At the high traffic load, the probability of large number of active users in a subframe may be large, which could oversteps the ability of multiple user detection, so these packets have to be discarded. Thus, in order to concisely describe the ability of multiple user detection, we can define a referential parameter $\theta = U_i/L$ as the overload rate of MPAD of the number of detected users in a subframe to the number of slots in a subframe, thus the maximum overload ratio $\theta_{\max}$ can be regarded as the control parameter for the MPAD, which can be utilized to denote how many collided packets of users can attempt to be recovered by using the MPAD. If $\theta \leq \theta_{\max}$ (i.e., $U_i \leq \theta_{\max} L$), the MPAD can be performed to detect collided packets in the i^{th} subframe. In realistic application, the parameter $\theta_{\max}$ can be selected according to the realistic decoding the ability of the MPAD.

It is assumed that the number of detected active users in the i^{th} subframe is U_i by performing preamble detection. The received symbol k^{th} in the i^{th} subframe can be denoted as

$$y_i(k) = \sum_{u=1}^{U_i} h_i^u S_i^u(k) z^{-\tau_{u,i}} + W_i(k). \tag{11}$$

It is assumed that the estimated channel coefficients and symbol-levels interleaver of the users in the i^{th} subframe are $\hat{h}_i^1, \ldots, \hat{h}_i^u, \ldots, \hat{h}_i^{U_i}$, and $I_1^s, \ldots, I_u^s, \ldots, I_{U_i}^s$, respectively. The bit-level interleaving operation can facilitate multiple user detection because it can lessen the relevance between adjoining bits. In addition, the zero padding and symbol level interleaving operation can lessen the complexity of MPAD and limit the number of superimposed symbol of activated devices. Considering above characteristics, we can use maximum a posteriori (MAP) to the proposed RIM scheme. However, to further lessen the detection complexity, the low-complexity message passing algorithm can be utilized to decode multiple collided packets by using the sparsity.

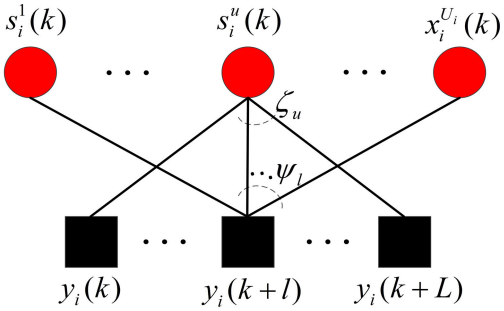

FIGURE 5. The factor graph model.

The Fig.5 shows a factor graph model with L function nodes and U_i variable nodes. The received every symbol from each L symbols in $\boldsymbol{Y}_i$ can be viewed as a function node, and the sent each symbol of each device can be viewed as a variable node. A edge from a function node to a variable node can be viewed as a detected grid mapping (i.e, zero padding and symbol interleaving). The MPAD can be iteratively carried out, and the extrinsic information of function node and variable node in the detector can be updated through the edge. For the $k-th$ symbol of the device u, the set of function nodes that are linked to the variable node $s_i^u(k)$ can be indicated as ζ_u. For the received signal $y_i(k+l)$ from the $l-th$ signal, the set of variable nodes that are linked to the function node $y_i(k+l)$ can be expressed as ψ_l. The factor graph of variable node $s_i^u(k)$ and function node $y_i(k+l)$ can be also presented in Fig.5. It can be defined respectively $\beta^t_{F_l->V_u}$ and $\beta^t_{V_u->F_l}$ as the transmitted message via edge from function node $y_i(k+l)$ to variable node $s_i^u(k)$ and from variable nodes $s_i^u(k)$ to function node $y_i(k+l)$ at the iteration t. It is assumed that the prior-probability can be equal. We initialize firstly the message from variable node $s_i^u(k)$ to function node $y_i(k+l)$, which is calculated as

$$\beta^0_{V_u->F_l} = \frac{1}{O}(l \in \zeta_u, for\ \forall u), \tag{12}$$

where O denotes the modulation order. Then update the message of function node $y_i(k+l)$ and variable node $s_i^u(k)$, which is expressed as

$$\begin{aligned}\beta^t_{F_n->V_l}(s_i^u(k) = \tilde{\boldsymbol{s}}_i^u) &= \sum_{x \in \boldsymbol{x}} \frac{1}{\sqrt{2\pi}\sigma} \exp\left(-\frac{1}{2\sigma^2}\left\| y_i(k+l) - \sum_{w \in \psi_l} h_i^u s_i^u(k)\right\|^2\right) \\ &\times \prod_{w \in \psi_l/\{u\}} \beta^{t-1}_{V_w->F_l}(s_i^u(k) = \tilde{\boldsymbol{s}}_i^u),\end{aligned} \tag{13}$$

and

$$\beta^t_{V_u->F_l}(s_i^u(k) = \tilde{\boldsymbol{s}}_i^u) = \prod_{m \in \zeta_u/\{l\}, x \in \tilde{\boldsymbol{s}}_i^u} \beta^{t-1}_{F_l->V_u}(s_i^u(k) = \tilde{\boldsymbol{s}}_i^u), \tag{14}$$

where $\tilde{s}_i^u$ represents a set with O modulated constellations. When $t = t_{\max}$, the symbol can be expressed as

$$\hat{s}_i^u(k) = \underset{\hat{S}_i^u(k)=S, S\in\boldsymbol{S}}{\arg\max} \left\{ \prod_{m\in\zeta_u} \beta_{F_m->V_u}^{t_{\max}}(\hat{S}_i^u(k)=S) \right\}. \quad (15)$$

Each packet replica contain L_{pay} payload symbols, so Eq.(12)-Eq.(15) are required to conduct L_{pay} times to obtain all estimated payload symbols.

Finally, according to the bit-level interleaver estimated by postamble detection, by using the bit-level deinterleaving operation, the estimated symbol $\hat{\boldsymbol{x}}_u$ of the $\hat{u}^{th}$ active user can be obtained. These estimated payload symbols are fed into a constellation demodulator and FEC decoder to obtain the payload bits of the $\hat{u}^{th}$ active user.

Note that the smaller ρ can result in the larger $\theta_{\max}$, the MPAD can detect more collided packets in a subframe. But the smaller ρ can result in the larger complexity and difficulty of detection, and the length of preamble should be larger to meet requirement of the detection. Therefore, the ρ can be practically chosen in line with the balance of the transmission requirement and the detection complexity.

IV. RIM-IRSA PROTOCOL

The RIM based RA framework provides a basic unit of multiple packets concurrence transmission, and is suitable to combine with the advanced RA protocol to further improve the throughput of RA system. Due to the high performance of IRSA, we employ IRSA protocol in the proposed RIM based RA framework, which can be termed as RIM-IRSA protocol. Since the basic transmission unit is different with that in the typical IRSA, the probability mass function of RIM-IRSA should be optimized.

The detailed processing flow of RIM-IRSA scheme is presented in Algorithm 1. At the gateway station, the MUD is carried out sub-frame by sub-frame within a frame. Note that once a packet replica is successfully decoded, its other packet replicas are removed by the IC processing. The RIM-IRSA protocol has a prominent advantage in which the iterative IC processing can allow more packet replicas to be decoded.

A. IMPLEMENTATION CONSIDERATION

In this section, the implementation consideration of RIM-IRSA protocol is shortly described, including the RIM-IRSA modulator and the RIM-IRSA demodulator.

The RIM-IRSA modulator is depicted in the upper part of Fig.6. In this modulator, the traffic packets queue of each active device is firstly segmented into fixed size MAC packets and buffered for transmission. Each MAC packet is copied into d replicas in a frame according to the optimal device degree distribution $\{\Lambda_d\}$, where Λ_d indicates the probability that a device sends d replicas, and these d replicas will be sent in randomly selected d slots within a frame. The signaling information that is used to indicate the location of slots to be sent is added to each packet replica. Then the payload bits of each packet replica are encoded and modulated by the FEC encoder and constellation modulator. After that, the interleaver is randomly selected by an active user, and the preamble is also randomly selected from the corresponding preamble set. The preamble set. The selected preamble is firstly added into each packet replica, then the data of each packet replica are mapped onto corresponding subframes according to its selected interleaver by a interleaver mapper. Finally, the signal of each replica is filtered through a square root raised cosine (SRRC) filter for transmission.

The RIM-IRSA demodulator is depicted in the lower part of Fig.6. The demodulator at the gateway station is carried out frame by frame. When the demodulator receives a frame signal from satellite node, it stores the samples of this frame signal in a cache device. The preamble detector is employed to perform preamble detection slot by slot. By preamble detection, the number of packet replicas in each slot can be determined. Then the MAC controller is conducted to judge whether a decoding condition is satisfied. If $\hat{K} \le \theta_{\max} L$, then MPAD detector is employed to decode these superimposed packets, otherwise, these packets are stored and continue to the next slot. After the MPAD, the constellation demodulator and FEC decoder are employed to obtain the effective information bits of the $\hat{K}$ packets. By cyclic redundancy check (CRC), if these packets are decoded successfully, the SIC

Algorithm 1 RIM-IRSA Demodulator.

Initialization: Initialize the number of time slot in a frame N_{slot};
Initialize the number of sub-frame in a frame N_{sf};
Initialize the pre-defined interleaver set and ρ, L, θ_{max}.

repeat
  for Each sub-frame $i^{th} \in [1, 2, \ldots, N_{sf}]$ **do**
    Estimate the number of user U_i in sub-frame i by using preamble detection;
    if $U_i \le \theta_{\max} L$ **then**
      Perform MPAD for the U_i devices;
      for Each device $\hat{u} \in [1, \ldots, U_i]$ **do**
        Estimate its interleaver and its preamble as Eq.(10);
        for Each symbol $k \in [1, \ldots, L_{pkt}^{RA}]$ **do**
          Estimate symbol $\hat{\boldsymbol{S}}_u(k)$ as Eq.(11) $\sim$ Eq.(15);
          Decode these packet replicas. If the decoding is successful, the IC technique is performed;
        end for
      end for
    else
      continue the next subframe;
    end if
  end for
until A maximum iterative time $I^{\max}$ has been achieved or none of packet is recovered.

Output: Payload bits of successfully recovered devices.

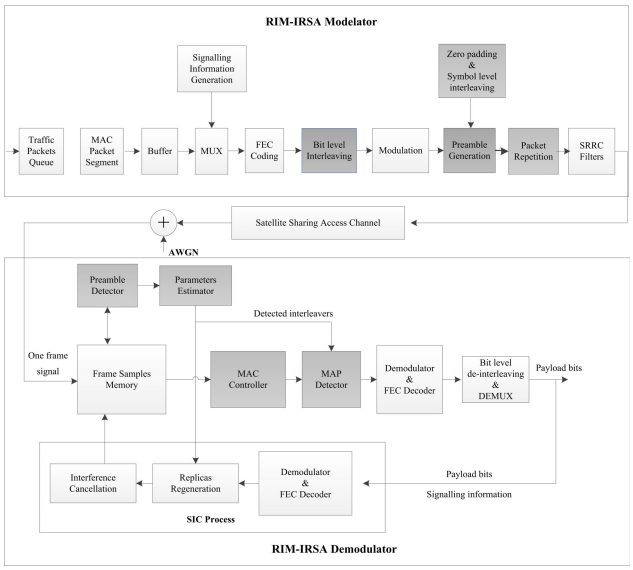

FIGURE 6. The baseband block diagram of the modulator and the demodulator of RIM-IRSA. In dark grey modified ones compared to the modulator and the demodulator of IRSA.

processor is employed to remove the interference contribution of their replicas in other slots in all sub-frames. The SIC processing is iteratively carried out until a maximum iterative times $I^{\max}$ has been reached or no packet replicas can be decoded.

Remarks: It is worth noting that many modern random access protocols usually use time slot based frame structure. The time slot frame information required for full network synchronization can be obtained through the broadcast information in satellite networks, and the overhead for full network synchronization is often transmitted in the broadcast channel. The frame structure of the proposed protocol is similar to those of traditional SA/CRDSA/IRSA protocols, which the packets are transmitted into slots randomly selected in a frame. In addition, the synchronous random access protocols indeed have higher overhead than the asynchronous protocols, but synchronous protocols have higher throughput performance than the asynchronous protocols. Thus, to further improve the throughput performance, we consider the synchronization RA system for the proposed scheme.

B. COMPUTATIONAL COMPLEXITY

Different from conventional IRSA, the complexity of the proposed protocol depends on preamble and the MPA detection. For preamble detection, the complexity is necessary to estimate interleaver and similar to convention IRSA scheme. For MPAD detection, the complexity can be denoted as $O(L_{pay}^{RA} O \cdot 2^{\bar{K}_{\max}})$, where $\bar{K}_{\max}(\bar{K}_{\max} \leq \theta_{\max} L)$ denotes the maximum decodable number of packets in a sub-frame. Moreover, the complexity of interference cancellation for every packet replica of RIM-IRSA can be similar to CRDSA/IRSA which the complexity gradually increases as load.

V. PERFORMANCE ANALYSIS

In this section, the theoretical PLR of RIM-IRSA is derived firstly by using density evolution analysis. Then the degree distribution optimization problem can be represented.

A. PLR ANALYSIS

We firstly bring in the concept of node degree distribution (i.e, the probability of how many edges a node owns) and edge degree distribution (i.e., the probability of how many an edge linked to a node). The node and edge degree distributions of a terminal node (TN) can be represented as

$$\Lambda(x) = \sum_d \Lambda_d x^d, \ \lambda(x) = \sum_d \lambda_d x^{d-1}, \tag{16}$$

where Λ_d represents the probability that a TN has d edges. $\lambda_d = d\Lambda_d / \sum_d d\Lambda_d$ represents the probability that an edge is linked to the TN with degree-d. The node and edge degree distribution of a subframe node (SN) can be represented as

$$\Psi(x) = \sum_l \Psi_l x^l, \rho(x) = \sum_l \rho_l x^{l-1}, \tag{17}$$

where Ψ_l indicates the probability that an SN owns l edges. $\rho_l = l\Psi_l / \sum_l l\Psi_l$ represents the probability that an edge is linked to the SN with degree-l.

Let $\varphi(r, \theta_{\max}, \rho)$ indicates the probability that a replicas can be straight detected as there has $r-1$ interfering replicas in the same subframe. Under the proposed MPA detector scheme, we assume that $r_{\max}$ indicates the maximum number of detecable replicas in a subframe. By utilizing tree analysis method [17], the density evolution equation that can be represented as

$$q_{i+1} = \sum_d \lambda_d p_i^{d-1} = \lambda(p_i), \tag{18}$$

$$\begin{aligned} p_i &= 1 - \sum_{l=1}^{\infty} \rho_l \sum_{r=1}^{l} \varphi(r, \theta_{\max}, \rho) \binom{l-1}{r-1} (1-q_i)^{l-r} (q_i)^{r-1} \\ &= 1 - e^{-q_i G \Lambda'(1)} \cdot \sum_{r=1}^{\infty} \frac{(q_i G \Lambda'(1))^{r-1}}{(r-1)} \varphi(r, \theta_{\max}, \rho). \end{aligned} \tag{19}$$

In RIM scheme, if $r \leq \theta_{\max} L$, r collided replicas can be successfully straight detected by utilizing the MPA detector. However, any replicas cannot be detected if the number of replicas in a subframe surpasses $\theta_{\max} L$. Therefore, for the convenience of analysis, $\varphi(r, \theta_{\max}, \rho)$ in proposed scheme can be calculated as

$$\varphi(r, \theta_{\max}, L) = \begin{cases} 1, & when\ r \leq \theta_{\max} L \\ 0, & when\ r > \theta_{\max} L. \end{cases} \tag{20}$$

If the number of slots in a MAC frame tends to infinity, there cannot be loops in a bipartite graph. By (18)-(20), the density evolution recursion for p_i can be further

indicate as

$$p_{i+1} = \begin{cases} 1 - e^{-\lambda(p_i)G\Lambda'(1)} \\ \cdot \sum_{r=1}^{\theta_{\max}L} \frac{(\lambda(p_i)G\Lambda'(1))^{r-1}}{(r-1)} & when\ r \le \theta_{\max}L \\ 0, & when\ \ r > \theta_{\max}L \end{cases}, \\ = f(p_i, G, \{\Lambda_l\}, \theta_{\max}, L). \quad (21)$$

In addition, q_0 can be initialized as 1, and p_0 is initialized by using Eq. (19). By putting p_0 into Eq. (21), the DE can be expressed as $f(p_I, G, \{\Lambda_d\}, \theta_{\max}, L)$. The asymptotic PLR can be indicate as

$$PLR(G,\{\Lambda_l\},\theta_{\max},L) = \sum\nolimits_d \Lambda_d (f(p_I,G,\{\Lambda_d\},\theta_{\max},L))^d. \quad (22)$$

and the throughput is indicate as

$$T = G[1 - PLR(G, \{\Lambda_d\}, \theta_{\max}, L)]. \quad (23)$$

B. DEGREE DISTRIBUTION OPTIMIZATION

In RIM-IRSA protocol, the user degree distribution of the conventional IRSA is no longer optimal due to considering RIM scheme and the multiple user detection algorithm. Based on the above derived PLR and throughput, the performance can be maximized by optimizing $\{\Lambda_d\}$. The maximization problem of throughput in RIM-IRSA can be indicate as,

$$\underset{\{\Lambda_d\}_{d=2}^{d_{\max}}}{\text{maximize}} \quad T{=}G[1{-}PLR(G,\{\Lambda_d\}_{d=2}^{d_{\max}},\theta_{\max},L)] \quad (24a)$$

$$\text{s.t. } PLR(G, \{\Lambda_d\}, \{\Gamma_l\}, L) < \overline{PLR} \quad (24b)$$

$$\sum\nolimits_{d=3}^{d_{max}} \Lambda_d = 1 \quad (24c)$$

$$0 \le \Lambda_d \le 1, \quad \forall d \in [2, \ldots, d_{max}], \quad (24d)$$

where the condition (24b) and (24c) indicate an upper bound $\overline{PLR}$ and the sum of all the probability levels of sent replicas. The (24d) indicates the range of Λ_d. By means of the differential evolution algorithm [18]-[19], the (24) can be resolved. The optimizing $\{\Lambda_d\}$ can make the throughput of RIM-IRSA be maximization.

VI. SIMULATION RESULTS

A. SIMULATION PARAMETERS

We adopt the MATLAB platform and Monte Carlo simulation method, and compare the throughput and PLR performance of SA, CRDSA, IRSA, RIM-SA and RIM-IRSA. The number of slots in each frame is $N_{slot} = 240$. The size of DFT and IFFT are 512 and 64, respectively. In addition, for a fair comparison with our proposed RIM-IRSA, we consider some typical RA scheme, such as SA, CRDSA, IRSA, and recent works NOMA-IRSA and non-orthogonal slotted ALOHA (NOSA) [23]. For NOMA-IRSA, the number of power level and target SINR are equal to 3 and 3 dB. For NOSA, it combines the CRDSA and sparse code multiple access (SCMA) technique to improve throughput performance in the satellite-enabled IoTs, which the protocol also apply code domain NOMA into RA system. The channel model and Rician factor are ITU-R M.1225 and 10dB, respectively. The simulation parameters are summarized in Table 1. Moreover, By using the differential evolution algorithm, we can obtain the optimal degree distributions of the proposed PM-IRSA protocol for different density parameters, which are summarized in Table 2.

TABLE 1. The simulation parameters.

Parameters	Values
The number of slot in a MAC frame, N_{slot}	240
Nomalized load, G	[0.1, 2.5]
Channel encode model	1/3 Turbo
The modulation order	4
Rician fator	10 dB
No. of Sub-carrier/IDFT size	512
Message Block Size/DFT size	64
Number of bits in a packet	1280
The maximum number of iterations,	15
Noise power spectral density,	-174 dBm/Hz

TABLE 2. The optimal degree distributions.

ρ	$\{\Lambda_d\}$
1/3	$\Lambda_1(x) = 0.841x^2 + 0.021x^3 + 0.138x^8$
1/4	$\Lambda_2(x) = 0.956x^2 + 0.044x^8$

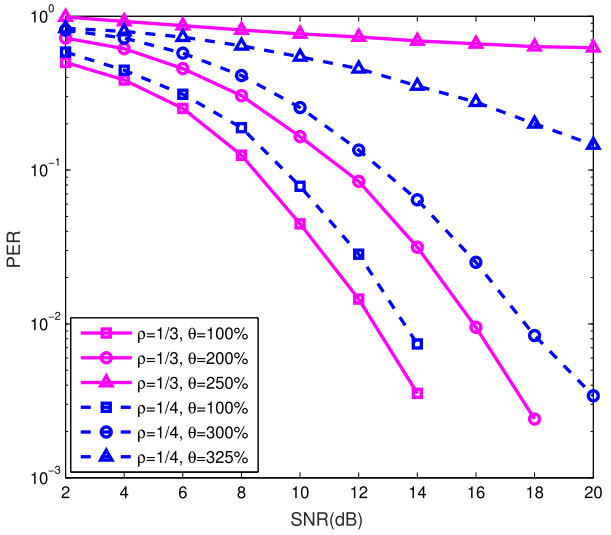

FIGURE 7. PER vs. SNR with different ρ and θ.

B. PERFORMANCE EVALUATION

We can see from Fig.7 that the packet error rate (PER) can achieve 0.01 at signal to noise rate (SNR) of 12.5 and 17.5dB for $\theta = 100\%$ and 200% when density $\rho = 1/3$, respectively. However, the PER cannot reach 0.01 for $\theta = 250\%$ when density $\rho = 1/4$. For RIM scheme with $\rho = 1/4$, the PERs reach 0.01 at SNR of 13.75dB and 16dB when $\theta = 100\%$ and 300% respectively, however the PER cannot achieve

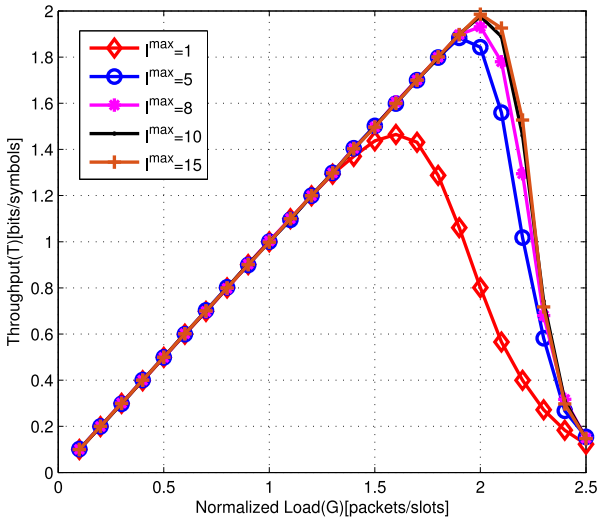

FIGURE 8. Normalized throughput vs. load with different iterative times.

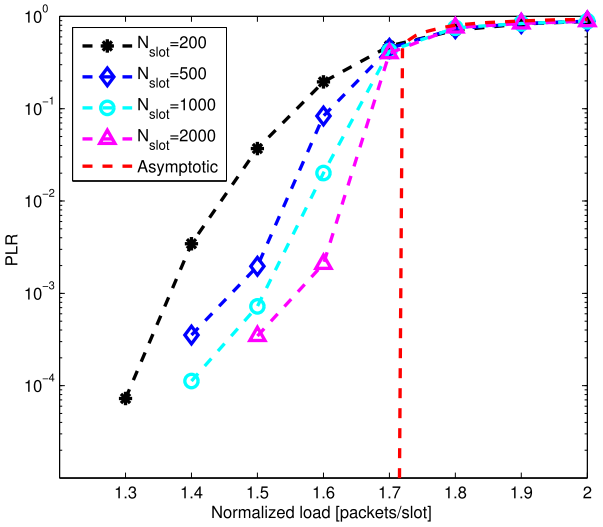

FIGURE 10. Asymptotic PLR of RIM-IRSA with $\rho = 1/4$.

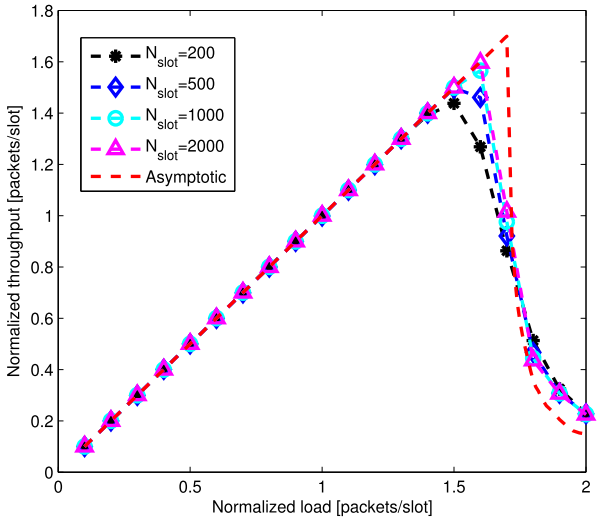

FIGURE 9. Asymptotic throughput of RIM-IRSA with $\rho = 1/4$.

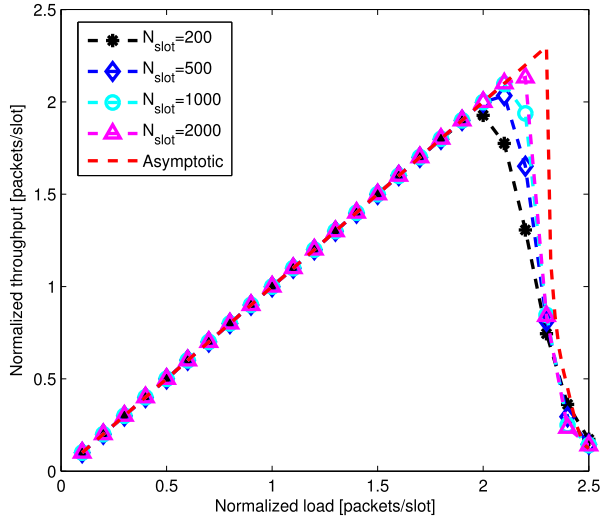

FIGURE 11. Asymptotic throughput of RIM-IRSA with $\rho = 1/3$.

0.01 when $\theta = 325\%$. These performance results can offer the reference about the setting of parameters of $\theta_{\max}$.

Considering MAC-layer simulation, the maximum overload ratios is $\theta_{\max} = 200\%, 300\%$ when density and $\rho = 1/3$, 1/4, respectively. The simulated throughput of the proposed protocol with $\rho = 1/3$ versus load with different iterative timesare plotted in Fig.8. It can be seen from Fig.8 that the throughput improvement is decreasing as I^{max} increases, and the performance can be converged when $I^{max} = 15$.

To study of asymptotic analysis results for the RIM-IRSA protocol with density and $\rho = 1/3$, 1/4, the asymptotic throughput and PLR and simulated ones with frame length $N_{slot} = 200, 500, 1000, 2000$ are given in Figs. 9-12, respectively. It can be seen from Fig.9 and Fig.10 the simulated ones can be slowly approach to the asymptotic ones as N grows when the density ρ equals 1/4. We can see form Fig.11 and Fig.12 that a similar trend with that in Fig. 9 and Fig.10 are presented, which justifies the correctness of asymptotic analysis for the proposed scheme. In addition, the asymptotic performances of the RIM-IRSA with $\rho = 1/4$ outperforms that of the RIM-IRSA with $\rho = 1/3$, which the reason is the multiple user detector can decode more collided packets in single subframe when $\rho = 1/4$.

The throughput versus load for the proposed protocol with $\rho = 1/3$ and 1/4, SA, CRDSA, IRSA with traditional degree distribution $\Lambda_c(x) = 0.5x^2 + 0.28x^3 + 0.22x^8$, NOSA and NOMA-IRSA with degree distribution $\Lambda_{noma}(x) = 0.761x^2 + 0.055x^3 + 0.022x^4 + 0.162x^8$ are respectively plotted in Fig.13. From Fig.13, we can see that the peak throughput of the RIM-IRSA with density $\rho = 1/4$ can reach about 2.0 packets/slot, which the proposed scheme can outperform conventional schemes and other recent works.

Fig.14 shows the PLR performances of these schemes. From Fig.14, we can see that the loads of RIM-IRSA with the density and $\rho = 1/3$, 1/4 can reach about

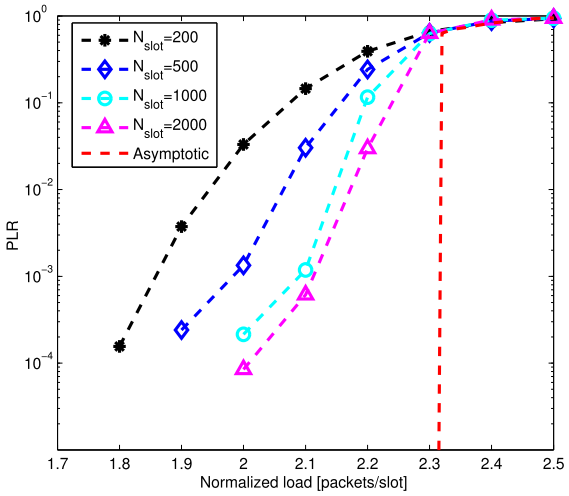

FIGURE 12. Asymptotic PLR of RIM-IRSA with $\rho = 1/3$.

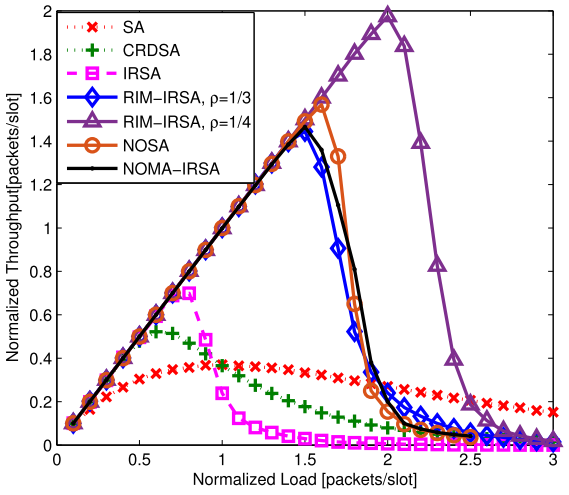

FIGURE 13. Normalized throughput vs. normalized load.

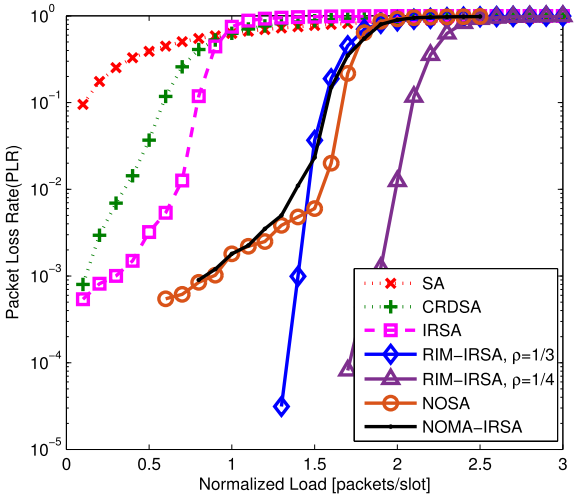

FIGURE 14. PLR vs. normalized load.

1.4 and 1.9 packets/slot when PLR equals 0.01, respectively. In addition, it can be seen that the proposed protocols with the density and $\rho = 1/3$, 1/4 have steeper regions of waterfall, which shows the better performance compared with conventional ones and other recent works.

VII. CONCLUSION

In this paper, we have proposed a RIM based random access framework for massive devices access into satellite-enabled IoT, and combine with the advanced IRSA protocol, dubbed RIM-IRSA. To maximize throughput performance of RA system with RIM-IRSA, the optimal degree distribution of RIM-IRSA can be obtain. Simulation results show that the performance of RIM-IRSA is much better than those of available SA, CRDSA, and IRSA, but its complexity is a slightly higher. The proposed RIM framework is a general framework, it can also be combined with the SA or CRDSA protocols, through their performances are lower than that of RIM-IRSA, their complexities are also lower. There is a challenge to combine the proposed RIM framework with the CSA protocol, which will bring further improvement of RA system, which is worthy to investigate in the future work.

ACKNOWLEDGMENT

This article was presented in part at the 2020 IEEE 91st Vehicular Technology Conference (VTC2020-Spring) [DOI: 10.1109/VTC2020-Spring48590.2020.9129425].

REFERENCES

[1] X. Li, Q. Liu, R. Yang, J. Wen, J. Zhang, E. Cai, and H. Zhang, "The combination of ground-sensing network and satellite remote sensing in Huailai county," *IEEE Sensors J.*, vol. 16, no. 10, pp. 3819–3826, May 2016.

[2] M. de Sanctis, E. Cianca, G. Araniti, I. Bisio, and R. Prasad, "Satellite communications supporting internet of remote things," *IEEE Internet Things J.*, vol. 3, no. 1, pp. 113–123, Feb. 2016.

[3] N. Celandroni and R. Secchi, "Suitability of DAMA and contention-based satellite access schemes for TCP traffic in mobile DVB-RCS," *IEEE Trans. Veh. Technol.*, vol. 58, no. 4, pp. 1836–1845, May 2009.

[4] W. Zhan and L. Dai, "Massive random access of machine-to-machine communications in LTE networks: Modeling and throughput optimization," *IEEE Trans. Wireless Commun.*, vol. 17, no. 4, pp. 2771–2785, Apr. 2018.

[5] R. De Gaudenzi, O. Del Rio Herrero, G. Gallinaro, S. Cioni, and P.-D. Arapoglou, "Random access schemes for satellite networks, from VSAT to M2M: A survey," *Int. J. Satell. Commun. Netw.*, vol. 36, no. 1, pp. 66–107, Dec. 2016.

[6] G. Choudhury and S. Rappaport, "Diversity ALOHA—A random access scheme for satellite communications," *IEEE Trans. Commun.*, vol. COM-31, no. 3, pp. 450–457, Mar. 1983.

[7] E. Casini, R. De Gaudenzi, and O. R. Herrero, "Contention resolution diversity slotted ALOHA (CRDSA): An enhanced random access scheme for satellite access packet networks," *IEEE Trans. Wireless Commun.*, vol. 6, no. 4, pp. 1408–1419, Apr. 2007.

[8] R. De Gaudenzi and O. R. del Herrero, "Advances in random access protocols for satellite networks," in *Proc. Int. Workshop Satell. Space Commun.*, Sep. 2009, pp. 331–336.

[9] G. Liva, "Graph-based analysis and optimization of contention resolution diversity slotted ALOHA," *IEEE Trans. Commun.*, vol. 59, no. 2, pp. 477–487, Feb. 2011.

[10] U. Demirhan and T. M. Duman, "Irregular repetition slotted ALOHA with energy harvesting nodes," *IEEE Trans. Wireless Commun.*, vol. 18, no. 9, pp. 4505–4517, Sep. 2019.

[11] F. Clazzer, E. Paolini, I. Mambelli, and C. Stefanovic, "Irregular repetition slotted ALOHA over the Rayleigh block fading channel with capture," in *Proc. IEEE Int. Conf. Commun. (ICC)*, May 2017, pp. 1–6.

[12] I. Hmedoush, C. Adjih, P. Mühlethaler, and L. Salaün, "Multi-power irregular repetition slotted ALOHA in heterogeneous IoT networks," in *Proc. 9th IFIP Int. Conf. Perform. Eval. Modeling Wireless Netw. (PEMWN)*, Dec. 2020, pp. 1–6.

[13] X. Shao, Z. Sun, M. Yang, S. Gu, and Q. Guo, "NOMA-based irregular repetition slotted ALOHA for satellite networks," *IEEE Commun. Lett.*, vol. 23, no. 4, pp. 624–627, Apr. 2019.
[14] J. Su, G. Ren, B. Zhao, and J. Ding, "Enhancing irregular repetition slotted ALOHA with polarization diversity in LEO satellite networks," *KSII Trans. Internet Inf. Syst.*, vol. 14, no. 9, pp. 3907–3923, 2020.
[15] E. Nisioti and N. Thomos, "Fast Q-learning for improved finite length performance of irregular repetition slotted ALOHA," *IEEE Trans. Cognit. Commun. Netw.*, vol. 6, no. 2, pp. 844–857, Jun. 2020.
[16] J. Su, G. Ren, and H. Zhang, "Random interleaving multiplexing based random access in IoT-oriented satellite networks," in *Proc. IEEE 91st Veh. Technol. Conf. (VTC-Spring)*, May 2020, pp. 1–5.
[17] M. Luby, M. Mitzenmacher, and A. Shokrollahi, "Analysis of random processes via and-or tree evaluation," in *Proc. 9th Annu. ACM-SIAM Symp. Discrete Algorithms*, San Francisco, CA, USA, Jan. 1998, pp. 364–373.
[18] R. Storn and K. Price, "Differential evolution—A simple and efficient heuristic for global optimization over continuous spaces," *J. Global Optim.*, vol. 11, no. 4, pp. 341–359, 1997.
[19] B. Zhao, G. Ren, X. Dong, and H. Zhang, "Optimal irregular repetition slotted ALOHA under total transmit power constraint in IoT-oriented satellite networks," *IEEE Internet Things J.*, vol. 7, no. 10, pp. 10465–10474, Oct. 2020.
[20] F. R. Kschischang and B. J. Frey, "Iterative decoding of compound codes by probability propagation in graphical models," *IEEE J. Sel. Areas Commun.*, vol. 16, no. 2, pp. 219–230, Feb. 1998.
[21] L. Yang, Y. Liu, and Y. Siu, "Low complexity message passing algorithm for SCMA system," *IEEE Commun. Lett.*, vol. 20, no. 12, pp. 2466–2469, Dec. 2016.
[22] X. Ma, L. Yang, Z. Chen, and Y. Siu, "Low complexity detection based on dynamic factor graph for SCMA systems," *IEEE Commun. Lett.*, vol. 21, no. 12, pp. 2666–2669, Dec. 2017.
[23] Q. Wang, G. Ren, S. Gao, and K. Wu, "A framework of non-orthogonal slotted ALOHA (NOSA) protocol for TDMA-based random multiple access in IoT-oriented satellite networks," *IEEE Access*, vol. 6, pp. 77542–77553, 2018.

JIAN DING was born in Henan, China, in 1987. He received the M.S. degree in electromagnetic theory and microwave engineering from China Research Institute of Radiowave Propagation, Qingdao, China, in 2012. He is currently pursuing the Ph.D. degree in communication and information systems with Xidian University, Xi'an, China. He is currently a Senior Engineer with China Research Institute of Radiowave Propagation. His research interests include wireless communication and random access technology.

JINGRUI SU (Graduate Student Member, IEEE) was born in Gansu, China, in 1990. He received the M.S. degree in instrumentation engineering from Xidian University, Xi'an, China, in 2016, where he is currently pursuing the Ph.D. degree in communication and information systems. His research interest includes random access technology in the IoT-oriented satellite networks.

CONG LI was born in Henan, China, in 1988. He received the Ph.D. degree in navigation guidance and control from Xidian University, Xi'an, China, in 2018. His research interest includes satellite intelligent communication.

GUANGLIANG REN (Member, IEEE) was born in Jiangsu, China, in 1971. He received the B.S. degree in communications engineering from Xidian University, Xi'an, China, in 1993, the M.S. degree in signal processing from the Academy of China Ordnance, Beijing, China, in 1996, and the Ph.D. degree in communications and information systems from Xidian University, in 2006. He is currently a Professor with the School of Telecommunications Engineering, Xidian University. He is the author of more than 40 research papers in journals and conference proceedings, such as IEEE TRANSACTIONS ON WIRELESS COMMUNICATIONS, IEEE TRANSACTIONS ON COMMUNICATIONS, and IEEE TRANSACTIONS ON VEHICULAR TECHNOLOGY, and the author or coauthor of three books. His research interests include wireless communications and digital signal processing, particularly multiple input multiple output (MIMO) systems, WiMax, and LTE.

HAO WANG was born in Shaanxi, China, in 1998. He received the B.S. degree in communications engineering from Xidian University, Xi'an, China, in 2020, where he is currently pursuing the M.S. degree in communication and information systems. His research interests include wireless communications and random access technology.